Saudi Journal of Biological Sciences 27 (2020) 706–712

Contents lists available at ScienceDirect

Saudi Journal of Biological Sciences

journal homepage: www.sciencedirect.com

Original article

Green synthesis and characterization of gold nanoparticles using endophytic fungi *Fusarium solani* and its in-vitro anticancer and biomedical applications

Prince Clarance [a], Ben Luvankar [a], Jerin Sales [a], Ameer Khusro [a], Paul Agastian [a], J.-C. Tack [b], Manal M. Al Khulaifi [c], Hind A. AL-Shwaiman [c], Abdallah M. Elgorban [c], Asad Syed [c], H.-J. Kim [b,*]

[a] Department of Plant Biology & Biotechnology, Loyola College, Chennai 600 034, Tamil Nadu, India
[b] Department of Clinical Pharmacology, College of Medicine, Soonchunhyang University, Cheonan, Republic of Korea
[c] Department of Botany and Microbiology, College of Science, King Saud University, P.O. Box 2455, Riyadh 11451, Saudi Arabia

ARTICLE INFO

Article history:
Received 14 November 2019
Revised 9 December 2019
Accepted 16 December 2019
Available online 24 December 2019

Keywords:
Chonemorpha fragrans
Camptothecin
Fusarium solani
Cytotoxicity
Cell cycle
DAPI staining

ABSTRACT

The present study aimed to explore the anticancer potentials of the gold nanoparticles (NPs) obtained by green synthesis method using an endophytic strain *Fusarium solani* ATLOY – 8 has been isolated from the plant *Chonemorpha fragrans.* The formation of the NPs was analyzed by UV, FTIR, SEM and XRD. The synthesized NPs showed pink-ruby red colors and high peak plasmon band was observed between 510 and 560 nm. It is observed that intensity of absorption steadily increases the wavelength and band stabilizes at 551 nm. The XRD pattern revealed the angles at 19, 38.32, 46.16, 57.50, and 76.81° respectively. Interestingly, the FTIR band absorption noted at 1413 cm^{-1}, 1041 cm^{-1} and 690 cm^{-1} ascribed the presence of amine II bands of protein, C-N and C-H stretching vibrations of the nanoparticles. SEM analysis indicated that the average diameter of the synthesized nanoparticles was between 40 and 45 nm. These NPs showed cytotoxicity on cervical cancer cells (He La) and against human breast cancer cells (MCF-7) and the NPs exhibited dose dependent cytotoxic effect. IC50 value was 0.8 ± 0.5 µg/mL on MCF-7 cell line and was found to be 1.3 ± 0.5 µg/mL on MCF-7 cell lines. The synthesized NPs induced apoptosis on these cancer cell lines. The accumulation of apoptotic cells decreased in sub G0 and G1 phase of cell cycle in the MCF-7 cancer cells were found to be 55.13%, 52.11% and 51.10% after 12 h exposure to different concentrations. The results altogether provide an apparent and versatile biomedical application for safer chemotherapeutic agent with little systemic toxicity.

1. Introduction

The synthesis of nanomaterials and nanoparticles emerged into a new era in biological research which has potential applications in biomedicine, pharmaceutical, biosensors, cosmetics, food technology, electronics, optical devices, dye degradation, wastewater treatment etc. (Bera and Belhaj, 2016; Fernandes et al., 2017; Frewer et al., 2014; Hussein, 2016; Sharif et al., 2017; Al-Dhabi et al., 2018a, 2019a). The enhanced property of nanoparticle depends on the size, distribution and morphology. The significant results can be obtained with nano dimensions ranged from 1 to 100 nm (Sivakumar et al., 2017; Arasu et al., 2017, 2019; Al-Dhabi et al., 2018b; Gurusamy et al., 2019; Rajkumari et al., 2019). Since gold nanoparticles are non-toxic and having high absorbance properties, it is widely used in various applications in health sector (Roopan et al., 2019; Valsalam et al., 2019a, 2019b). Many authors have reported that gold nanoparticles are an ideal source for biosensors and appropriate agent to kill cancer cells (Huang et al., 2006; Huff et al., 2007; Arokiyaraj et al., 2015). The synthesis of NPs by biological method involving green-chemistry, eco-friendly based approach, make use of the active compounds of plants, bacteria, fungi, actinomycetes, yeast and algae (Li et al., 2011; Shankar et al., 2003). Endophytic organisms have many associations with host plants and are survive in the inner wall of healthy plants. These endophytic organisms have lot of potentials

* Corresponding author.
E-mail addresses: hak3962@sch.ac.kr, hakkimabcd@gmail.com (H.-J. Kim).
Peer review under responsibility of King Saud University.

Production and hosting by Elsevier

https://doi.org/10.1016/j.sjbs.2019.12.026
1319-562X/

to synthesize antibacterial, anti-oxidant, antiviral, immunosuppressant and insulin mimetic properties. In a study, (Shankar et al., 2003) reported the application of *Pelargonium graveolens* leaves and its associated endophytic strains in gold NPs synthesis. Also, *Amylomyces rouxii*, an endophytic fungus has been utilized for the synthesis of silver NPs synthesis (Musarrat et al., 2010). These green synthesized NPs have lot of potentials against various Gram-positive, Gram-negative, phytopathogenic and human pathogenic fungi (Verma et al., 2011; Raheman et al., 2011). Likewise, (Devi et al., 2012) isolated an endophytic *Penicillium* sp. from the medicinal plant, *Centella asiatica* for the synthesis of silver NPs. The green synthesized NPs showed potential antibacterial activity against various human pathogens. In this study, we screened endophytic fungi extracts for the synthesis of gold NPs and characterized. We also investigated the particle size of synthesized NPs and structural characterization was performed. The cytotoxic effect of the NPs was also studied on breast cancer cells.

2. Materials and methods

2.1. Collection of plant materials

Chonemorpha fragrans belongs to the family *Apocynaceae*. It is a large woody climber and found in the Western Ghat regions of Kerala. Roots of the plant produce highest levels of CPT than bark and stem (Kedari and Malpathak, 2013). Mature plant parts including roots and transition zones were collected. It was placed in sterilized polypropylene covers and transported to the laboratory. The selected medicinal plant was identified by authenticated taxonomist Dr. G. Jeyajothi from the department. We have deposited the voucher specimen in this department (specimen number: 314) for future reference.

2.2. Isolation of endophytic fungus

In this study, explants were used for the isolation of endophytic fungus as suggested by (Hallmann et al., 2006) with little modifications. Briefly, roots were carefully rinsed with 0.1% (v/v) Tween 20 (30 s) and 0.1% (v/v) Bevistin (60–180 s) to avoid fungal growth on explants. Then it was immersed in sodium hypochlorite solution (0.1%, v/v) (30 s) and treated with ethanol (70%, v/v) (3–5 min). The sample was rinsed with double distilled water before to start each experimental procedure. Then the disinfected sample was dried in a Laminar air flow cabinet aseptically and exposed cortex region. Further, it was kept on agar medium for the isolation of endophytic fungi. All plates were incubated at 28 ± 2 °C for 5–7 days under dark. After one week, a single hyphal tip was carefully separated from the plate and further sub cultured on potato dextrose agar plates (Himedia, Mumbai, India) and incubated for 5 days at 28 ± 2 °C. The isolated culture was stored as slants and also stored in glycerol (50%, v/v) at −80 °C.

2.3. Molecular characterization of endophytic fungus

The isolated fungus was characterized based on 18S rDNA gene sequencing. DNA of the fungus was extracted using a DNA isolation kit as per manufacturer's instructions. The internal transcribed regions of 18S rDNA were amplified using ITS4 and ITS1 region (Innis et al., 1990). The amplified 18S rDNA gene sequences were submitted after the analysis of Basic local alignment search tool (BLAST).

2.4. Green synthesis of gold NPs

In this study, the isolated *Fusarium solani* was cultured in YEPD broth and the culture was kept on a shaker incubator at 120 rpm (28 °C). The culture was incubated up to 9 days and the culture was filtered using a cheese cloth and washed with double distilled water sever times. To the biomass, 100 ml sterile milli Q water was added and kept in static condition for 2 days. Then the total biomass was passed through Whatman No-1 filter paper. Then the pH of the sample was maintained as 8.5 using 0.1 N NaOH. About 1 mM $HAuCl_4$ (99 ml) solution was taken in a clean beaker, to this 1.0 ml fungal extract was added and incubated for 48 h under dark (Figure not shown).

2.5. Characterization of gold nanoparticles

The green synthesized NPs were characterized using UV–Visible spectrophometer between wavelength 350 and 800 nm. The peak value towards these ranges was tested. FT-IR analysis (Perkin-Elmer) was also performed to analyze the functional groups of NPs. These two analyses were performed periodically to monitor the development of NPs. X-Ray diffraction (XRD) analysis (Philips PW 1830 instrument) and particle size analysis (Malvern Zetasizer-nanosizer) were used to characterize NPs.

2.6. Cell culture and maintenance

Anticancer properties of NPs on Human embryonic kidney (HEK) cells, cervical cancer (HeLa) cells and Human Breast (MCF-7) were analyzed. Bacterial and fungal contaminations were restricted by adding streptomycin and penicillin (100 IU/100 μg) with this medium. All three cell lines were cultured at 37 °C in the presence of 5% CO_2 using a CO_2 incubator in a standard method (Thangam et al., 2011; Vivek et al., 2011).

2.6.1. Evaluation of cytotoxicity

MTT assay was performed to analyze the inhibitory concentration (IC_{50}) of synthesized NPs. Initially all three cancer cell lines were culture in a microtitre plant for about 2 days to obtain 75% confluence. The medium was discarded and MTT was added on the culture and incubated for 4 h at 37 °C. Then, the supernatant was removed and about 50 μL of DMSO was loaded with the sample and incubated for 10 min. The absorbance was read at 620 nm using a microtitre plate reader and the percentage viability was calculated.

2.6.2. Morphological assays

For the morphological assay, MCF-7 cells were treated with NPs at various concentrations and further fixed using ethanol and acidic acid solution at the ratio of 3:1 (v/v). Further, the cover slip was carefully mounted on a glass slide to analyze morphological changes.

2.6.2.1. Apoptotic cell death analysis. The MCF-7 cell line concentration was adjusted as 1×10^5 cells/mL before to perform the experiment. To the 90 μL MCF-7 cells, 1 μL dye (mg/ml ethidium bromide and acridine orange) was mixed on cover slips.

2.6.2.2. DAPI nuclear staining. In this study, the MCF-7 cells were placed on coverslip using a 24-well microtiter plate with NPs for 24 h. The fixed MCF-7 cells were incubated with triton X-100 and allowed for permeation for 3 min. Then DAPI (10 μL) was added over the cell lines and the cells were analyzed under a fluorescent microscope (Nikon Eclipse, Inc, Japan).

2.7. Cell cycle analysis

Cell cycle was analyzed to evaluate the impact of NPs on the mechanism of green synthesized NPs mediated cell changes. Two cancer cell lines (MCF-7 and HeLa cells) were subjected for cell

cycle analysis. A flow cytometry was used to analyze the cell cycle (BD FACS flow cytometer) and the intensity of fluorescent signal was observed by CellQuest and Modifit.

2.8. Statistical analysis

All analytical experiments were carried out in triplicate experiments. The analytical results were analyzed using SPSS (version 17.0) statistical software. The *P*-value (<0.01) was described as statistical significant.

3. Results and discussion

3.1. Isolation of endophytic fungi

The fungi showed a white cottony growth on PDA covering the entire plate within 6–7 days. The hyphae appeared as hyaline hyphae and yellowish mycelium was observed, then the colour of the mycelium changed as bluish –grey after 14 days of incubation. The amplified gene product was purified using agarose gel electrophoresis and 476 bp amplicon was observed.

3.2. ITS rDNA sequencing

The ITS region of rDNA sequence data of the fungus gave 100 percent similarity for the fungus in the NCBI GenBank database and identified as *Fusarium solani* ATLOY-8. The 18S rDNA sequence was finally deposited in Genbank with Accession No, KY497951. The 18S rDNA sequence of *Fusarium solani*ATLOY-8 was compared and phylogentic tree was constructed.

3.3. XRD and FT-IR studies

Camptothecin stabilized gold nanoparticles were successfully synthesized by the above mentioned modified method. Fig. 1 represents the XRD analysis of Camptothecin stabilized gold NPs which produced by *Fusarium solani* associated with *Chonemorpha fragrans*. Crystalline structure and phase purity of the synthesized nanoparticles were analysed usingX-ray Diffraction studies. The diffraction pattern was analysed in the range of 2θ between 5 and 80°. Fig. 1 shows the p-XRD patterns of CPT (Camptothecin) with Gold nanoparticles under optimum conditions are shown. Peaks at angles at 2θ = 32. 19, 38. 32, 46.16, 57.50, and 76.81° shows distinct peaks of CPT with gold nanoparticles. The diffraction peaks were indexed as (0 0 6), (1 1 1), (2 0 0), (2 2 0), (3 1 1) which suggested the reflections of gold NPs. CPT stabilized AuNPs did not change any shift patterns. Thus CPT coating did not affect the integrity of the structure of Au NPs was stabilized by CPT.

Fig. 2 shows the FT- IR spectrum of synthesized gold nanoparticles. The spectrum showed different IR peaks at different positions for various functional groups. The peaks at 1413 cm^{-1} ascribed to the amine II bands of protein present in the sample. The observed band at 1041 cm^{-1} corresponds to the C-N stretching vibrations. The band obtained at 690 cm^{-1} revealed C-H stretching vibrations. These bands revealed the presence of amide II bands of proteins and or/ polypeptides respectively. These findings were highly agreed with previous findings (Caruso et al., 1998; Van de Weert et al., 2001).

3.4. UV–Visible spectroscopy

The stabilization of gold nanoparticles by camptothecin was analyzed by the UV – Visible spectroscopy. The UV–Visible spectra of gold NPs stabilized using camptothecin were presented in Fig. 3. The synthesized NPs showed pink-ruby red colors and high peak plasmon band was observed between 510 and 560 nm. It is observed that intensity of absorption steadily increases the wavelength and band stabilizes at 551 nm. This finding is in good agreement with the previously reported values (Mulvaney, 1996). The exhibited high absorption band at 545 nm attributed to the formation of camptothecin loaded Gold nanoparticles. Single and intense absorption peak in the spectra confirm the formation of metallic gold nanoparticles. No additional peaks or shoulder peaks were found in the spectra proves that all camptothecin loaded gold solution reduced to metallic gold and none left un-reacted.

3.5. SEM, DLS and zeta potential studies

The morphological study of synthesized Camptothecin loaded gold nanoparticles was analyzed by SEM analysis. Fig. 4 shows the SEM image of gold nanoparticles which was stabilized by using camptothecin. The obtained images were found to be needle and flower like structures with spindle shape. The nanoparticles are aggregated and agglomerated in the observed SEM images. DLS analysis was applied to measure the particle size of the synthesized camptothecin stabilized gold nanoparticles. Fig. 5 shows the particle size distribution of Camptothecin stabilized NPs. The average diameter of the synthesized nanoparticles between 40 and 45 nm. The present finding revealed that, CPT is the most stabilizing agent which gave rise to nanosized gold nanoparticles. Particle stability and adhesion of the synthesized NPs are significantly

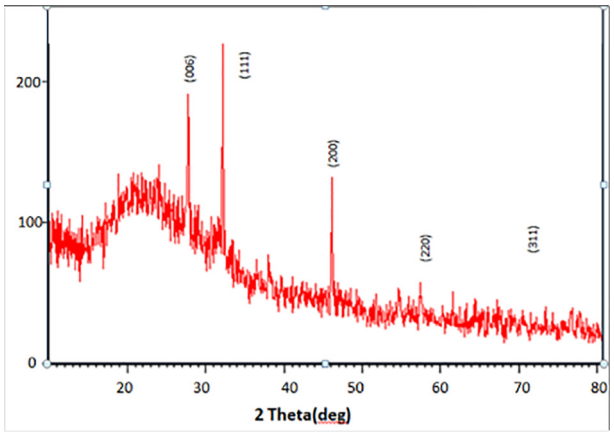

Fig. 1. XRD pattern of Camptothecin loaded gold nanoparticles.

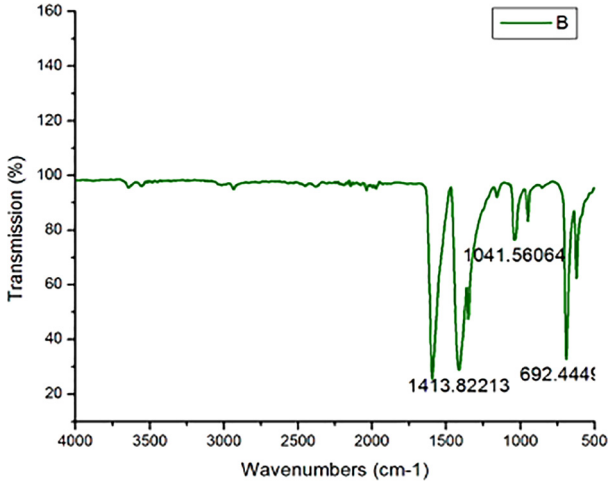

Fig. 2. FT-IR studies of Camptothecin loaded gold nanoparticles.

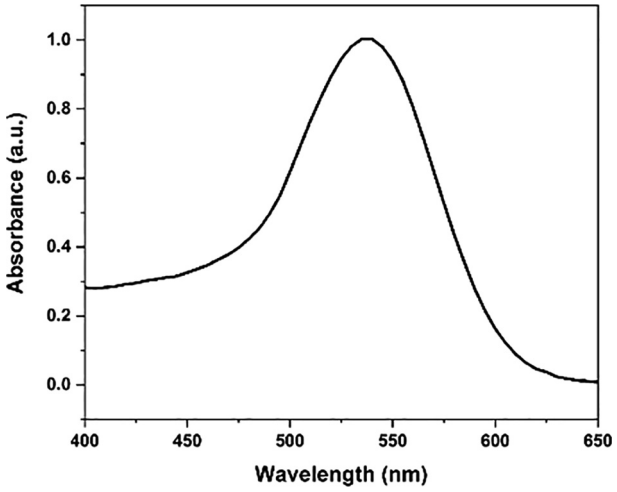

Fig. 3. UV–Visible spectra of Camptothecin loaded gold nanoparticles.

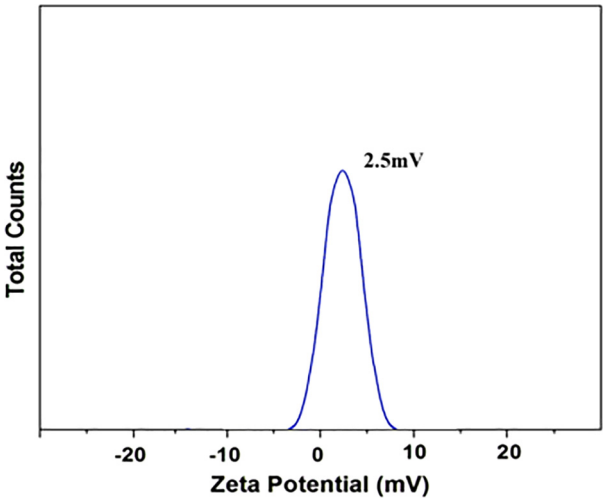

Fig. 6. Zeta potential studies Camptothecin loaded gold nanoparticles.

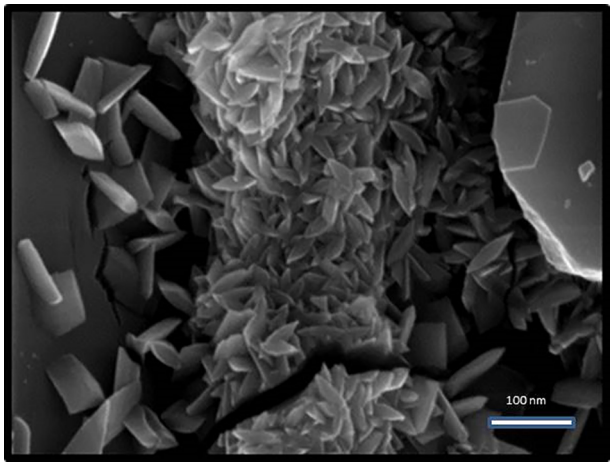

Fig. 4. SEM image of Camptothecin loaded gold nanoparticles.

influenced by the zeta potential. Fig. 6 showed the charge reversal behaviour of gold nanoparticles which was inferred by difference in zeta potential value. The zeta potential value of gold nanoparticles undergone charge transition, from negative (−3.00) to positive (7.00). The zeta potential of gold nanoparticles at 25 °C was observed as 2.5 mV, which mainly indicates the stability of the NPs in aqueous (water) solution. Because of the aggregation of particles, the repulsion between the particles get reduced thus decrease the stability of the particles (Rahme et al., 2013).

3.6. Cytotoxicity assay

3.6.1. MTT assay

The synthesized Nano particles on the cell response of MCF-7, HeLa and Human Embryonic Kidney cell line using MTT assay was examined and IC_{50} values were calculated and shown in Table 1. The results indicate anticancer potential of NPs on HeLa cell lines and the IC_{50} value was found to be 1.3 ± 1.0 μg/ml followed by 0.8 ± 0.5 μg/ml against MCF-7 cell line. It can be noticed from the results that there was an insignificant activity found in Human Embryonic Kidney (HEK) cell line shown in Fig. 7. The morphology of the MCF-7 cells in the presence and absence of NPs was also studied using inverted phase contrast microscopy. The results were shown in Fig. 8. In the control, high density of cell layer was observed. Cells treated with synthesized nanoparticles were observed with low density, more condensed, irregular and fragmented in MCF-7 cells lines due to apoptotic cell death. It is stated

Table 1
Cytotoxic activity of sample (μg/ml).

Cells	IC_{50}
MCF-7	0.8 ± 0.5
HeLa	1.3 ± 1.0
HEK	Insignificant toxicity

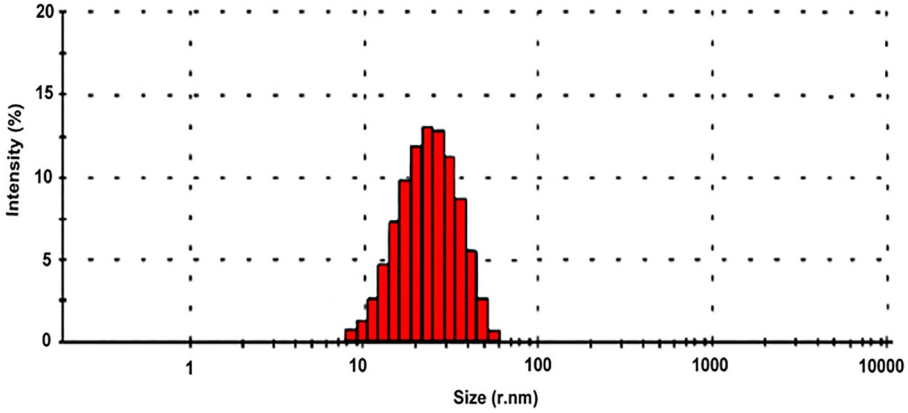

Fig. 5. Particle size distribution of Camptothecin loaded gold nanoparticles.

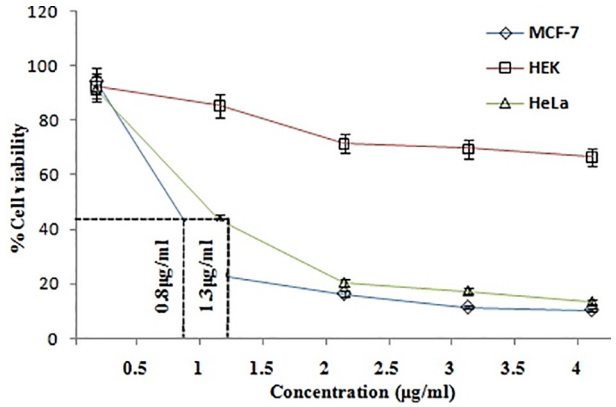

Fig. 7. The cytotoxic effect of MTT reduction assay showing the IC_{50} values in MCF-7, HeLa and insignificant cytotoxic effect of HEK cells on camptothecin loaded gold nanoparticles.

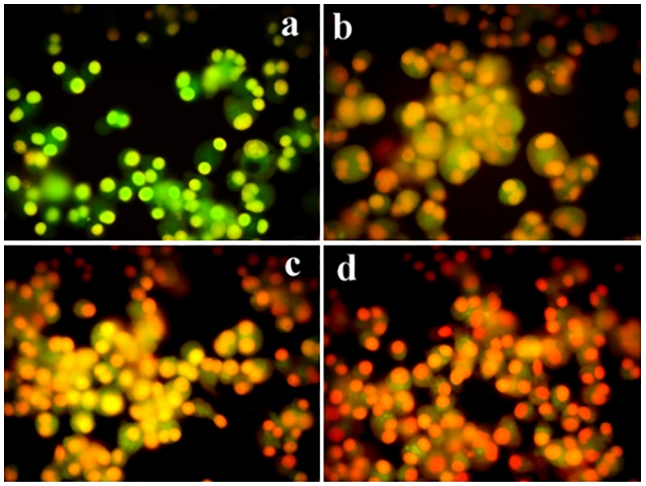

Fig. 9. MCF-7 cells treated with different concentrations of (0.5 µg/ml, 1 µg/ml, and 2 µg/ml) of the $HAuCl_4$ solutionand further stained with AO/EtBr (b-d). a – control.

that after exposure to light of an appropriate wavelength, NPs are being led to the generation of cytotoxic reactive oxygen species (ROS) (Valsalam et al., 2019; Anju et al., 2019). Bao et al. (2016) reported that, 10-hydroxycamptothecin-conjucated gold nanoparticles showed potent cytotoxicity against MDA-MB-231 cell lines. It is because the ROS leads to microbial cell death and cell damage (Parasuraman et al., 2018; 2019a, 2019b).

3.6.2. Acridine orange/EtBr staining

The AO/EtBr staining results revealed apoptotic cell death due to the activity of NPs (Fig. 9). The untreated cancer cells (control) did not show any significant adverse effects. Where MCF-7 cell line appeared dense red colour, which is mainly due to apoptotic cell death and results highly condensed nuclear materials. Previously (Singh et al., 2013) used green synthesized gold NPs from *Padina gymnospora* and reported irregular size, plasma membrane blebbingand mitochondrial depolarization in apoptotic cell death of HepG2 and A549 cells. There are several authors reported that when cells undergoing for an apoptotic death, the DNA in cells becomes as dense, fragmented and condensed chromatin (Manivasagan and Oh, 2015; Park et al., 2017).

3.6.3. DAPI staining

The DAPI staining method was used to evaluate to check the nuclear fragmentation and condensation of nanoparticle treated cell lines. There are no significant changes observed in untreated cells at 400× magnification under fluorescence microscope. The nanoparticle treated cancer cell lines of MCF-7 cells show bright patches which indicates the condensed chromatins and nuclear fragmentations shown in Fig. 10. HeLa cells were treated with novel fucoidanase Gold Nanoparticles induced the DNA damage and apoptosis in cancer cells were reported by (Acevedo-Morantes et al., 2013) Loss of morphological feature was observed after 10 h of treatment of MCF7 cells at low concentrations of Camptothecin: SLN complexes (Marzouni et al., 2018).

3.6.4. Cell cycle arrest analysis

To explore the mechanism of synthesized green nanoparticles mediated cell changes, we analysed the cells after 12 h exposure of the cells with synthesized GNPs (Fig. 11). We found that there was accumulation of cells in the G0-G1, S and G2/M-phase of control cells. There were no changes in the G0-G1-phase and the percentage of cells was remaining constant. Apoptosis can be induced by arrest of cell cycle. Accumulation of apoptotic cells decreased in sub G0 and G1 phase of cell cycle in the MCF-7 cancer cells were found to be 55.13%, 52.11% and 51.10% after 12 h exposure to different concentrations of 0.5 µg/ml, 1 µg/ml, and 2 µg/ml of the extract respectively (c-d, and a is control) as compared to the

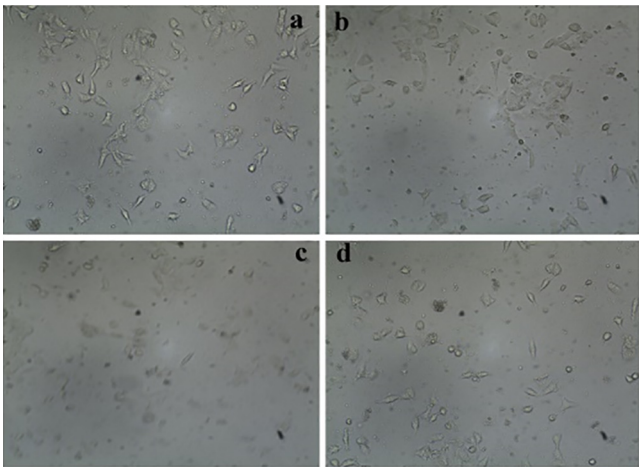

Fig. 8. The morphological characterization of MCF-7 cells treated (b-d treated) with 0.5 µg/ml, 1 µg/ml, and 2 µg/ml, of $HAuCl_4$ solutionrespectively and (a) control.

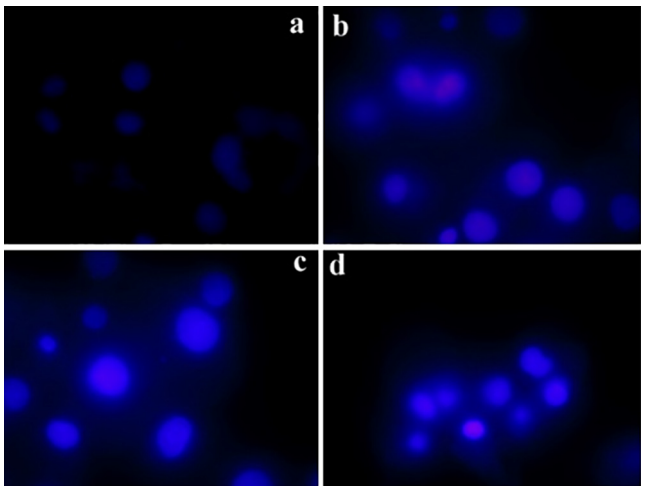

Fig. 10. MCF-7 cells treated with different concentrations of (0.5 µg/ml, 1 µg/ml, and 2 µg/ml) of the $HAuCl_4$ solution and further stained with the nuclear stain DAPI.

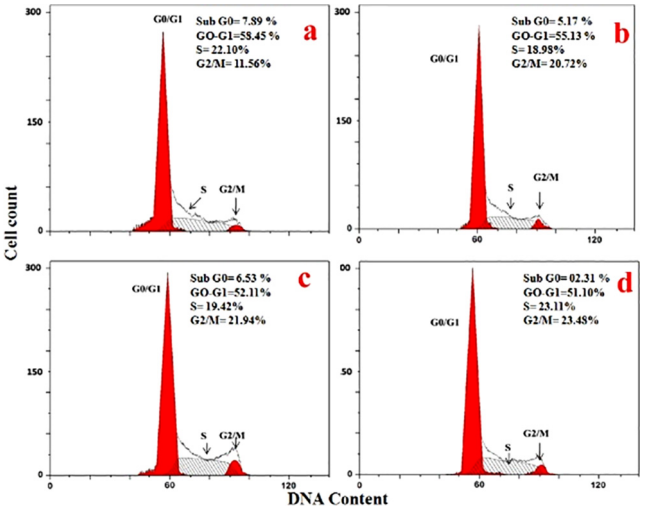

Fig. 11. $HAuCl_4$ solutiontreated in different concentration of 0.5 μg/ml, 1 μg/ml, and 2 μg/ml inMCF-7 cells (b-d). a – control, and further stained with PI for cell cycle analysis by flow cytometry. Panels indicate the occurrence of cells in each phase of the cell cycle. Data show the percentage of live cells in each phase of the cell cycle.

control. This was due to the inhibition of cyclin expressions. Cyclins are the most important protein involved in the G1 to S transition of the cell cycle.

We observed the reduction of G2 and M phase simultaneously which indicated significant arrest of cell cycle check point G1/S transition phase. Many others reported that decrease of cyclin plays a vital role in apoptotic cell death. It was previously reported the influence of gold nanoparticles green synthesized by *Abutilon indicum* on HT-29 colon cancer cells (Mata et al., 2016).

4. Conclusion

The present finding represents a very efficient and environment friendly method of the synthesis of gold nanoparticles using crude extract of an endophytic fungus from the plant roots of *Chonemorpha fragrans.* The fugal aqueous filtrate mediated the production of gold nanoparticles between 40 and 45 nm. The synthesized gold nanoparticles were characterized by various analytical techniques and the synthesized particles found to be highly stable. The biosynthesized gold nanoparticles have shown effective anticancer activities. These gold nanoparticles showed potent cytotoxic agents on MCF-7 and HeLa cells**.** This alternative method of biosynthesis of gold nanoparticles would stand against the popular chemical methods in the field of medical biotechnology.

Acknowledgement

The authors extend their appreciation to the Deanship of Scientific Research at King Saud University for funding this work through research group No (RG-1440-056). The authors thank Loyola college for the support for the performance of the work. The authors Hak-Jae Kim thank the support received from Soochunhyang University research fund for this research work.

References

Acevedo-Morantes, C.Y., Acevedo-Morantes, M.T., Suleiman-Rosado, D., Ramírez-Vick, J.E., 2013. Evaluation of the cytotoxic effect of camptothecin solid lipid nanoparticles on MCF7 cells. Drug. Deliv. 20, 338–348.

Al-Dhabi, N.A., Ghilan, A.-K.M., Arasu, M.V., 2018b. Characterization of silver nanomaterials derived from marine streptomyces sp. Al-Dhabi-87 and its in vitro application against multidrug resistant and extended-spectrum beta-lactamase clinical pathogens. Nanomaterials 8 (5).

Al-Dhabi, N.A., Ghilan, A.K.M., Arasu, M.V., Duraipandiyan, V., Ponmurugan, K., 2018a. Environmental friendly synthesis of silver nanomaterials from the promising Streptomyces parvus strain Al-Dhabi-91 recovered from the Saudi Arabian marine regions for antimicrobial and antioxidant properties. J. Photochem. Photobiol., B 189, 176–184.

Al-Dhabi, N.A., Ghilan, A.K.M., Arasu, M.V., 2019a. Duraipandiyan V. Green biosynthesis of silver nanoparticles produced from marine *Streptomyces* sp. Al-Dhabi-89 and their potential applications against wound infection and drug resistant clinical pathogens. J. Photochem. Photobiol., B. 111529.

Anju, V.T., Parasuraman, P., Lal, S.S.B., Sharan, A., Syed, A., Bahkali, N.A., Alsaedi, M. H., Kasinathan, K., Busi, S., 2019. Antimicrobial photodynamic activity of toluidine blue-carbon nanotube conjugate against *Pseudomonas aeruginosa* and Staphylococcus aureus - Understanding the mechanism of action. Photodiagnosis. Photodyn. Ther. 27, 305–316.

Arasu, M.V., Thirumamagal, R., Srinivasan, M.P., Al-Dhabi, N.A., Ayeshamariam, A., Saravana Kumar, D., Punithavel, N., Jayachandran, M., 2017. Green chemical approach towards the synthesis of CeO2 doped with seashell and its bacterial applications intermediated with fruit extracts. J. Photochem. Photobiol., B 172, 50–60.

Arasu, M.V., Arokiyaraj, S., Viayaraghavan, P., Kumar, T.S.J., Duraipandiyan, V., Al-Dhabi, N.A., Kaviyarasu, K., 2019. One step green synthesis of larvicidal, and azo dye degrading antibacterial nanoparticles by response surface methodology. J. Photochem. Photobiol., B 190, 154–162.

Arokiyaraj, S., Saravanan, M., Badathala, V., 2015. Green synthesis of Silver nanoparticles using aqueous extract of Taraxacum officinale and its antimicrobial activity. South Indian J. Biol. Sci. 2, 115–118.

Bao, H., Zhang, Q., Xu, H., Yan, Z., 2016. Effects of nanoparticle size on antitumor activity of 10-hydroxycamptothecin-conjugated gold nanoparticles: in vitro and in vivo studies. Int. J. Nanomed. 11, 929–940.

Bera, A., Belhaj, H., 2016. Application of nanotechnology by means of nanoparticles and nanodispersions in oil recovery - a comprehensive review. J. Nat. GasSci. Eng. 34, 1284–1309.

Caruso, F., Furlong, D.N., Ariga, K., Ichinose, I., Kunitake, T., 1998. Characterization of polyelectrolyte−protein multilayer films by atomic force microscopy, scanning electron microscopy, and Fourier transform infrared reflection−absorption spectroscopy. Langmuir 14, 4559–4565.

Devi, N.N., Shankar, D.P., Sadhasivam, S., 2012. Biomimetic synthesis of silver nanoparticles from an endophytic fungus and their antimicrobial efficacy. Int. J. Biomed. Adv. Res. 3, 409–415.

Fernandes, C., Benfeito, S., Fonseca, A., Oliveira, C., Garrido, J.E.M., 2017. Photodamage and photoprotection: toward safety and sustainability through nanotechnology solutions. Nanotechnol. Agri-food Ind., 527–565

Frewer, L.J., Gupta, N., George, S., Fischer, A.R.H., Giles, E.L., Coles, D., 2014. Consumer attitudes towards nanotechnologies applied to food production. Trends Food Sci. Technol. 40, 211–225.

Gurusamy, S., Kulanthaisamy, M.R., Hari, D.G., Veleeswaran, A., Thulasinathan, B., Muthuramalingam, J.B., Balasubramani, R., Chang, S.W., Arasu, M.V., Al-Dhabi, N.A., Selvaraj, A., Alagarsamy, A., 2019. Environmental friendly synthesis of TiO2-ZnO nanocomposite catalyst and silver nanomaterials for the enhanced production of biodiesel from Ulva lactuca seaweed and potential antimicrobial properties against the microbial pathogens. J. Photochem. Photobiol., B 193, 118–130.

Hallmann, J., Berg, G., Schulz, B., 2006. Isolation procedure for endophytic microorganisms. In: Boyle, Sieber, Ch, J.C., Schulz, T.N., B.J.E. (Eds.), Microbial Root Endophytes. Springer, Berlin. Heidelberg, pp. 299–305.

Huang, X., El-Sayed, I.H., Qian, W., El-Sayed, M.A., 2006. Cancer cell imaging and photothermal therapy in the near-infrared region by using gold nanorods. J. Am. Chem. Soc. 128, 2115–2120.

Huff, T.B., Tong, L., Zhao, Y., Hansen, M.N., Cheng, J.X., Wei, A., 2007. Hyperthermic effects of gold nanorods on tumor cells. Nanomedicine (Lond). 2, 125–132.

Hussein, A.K., 2016. Applications of nanotechnology to improve the performance of solar collectors – recent advances and overview. Renew. Sust. Energ. Rev. 62, 767–792.

Innis, M.A. (Ed.), 1990. PCR Protocols: A Guide to Methods and Applications. Academic Press, p. 482.

Kedari, P., Malpathak, N., 2013. Subcellular Localization and quantification of camptothecin in different plant parts of *Chonemorphafragrans*. Adv. in Zool. and Bot. 1, 34–38.

Li, X., Xu, H., Chen, Z.-S., Chen, G., 2011. Biosynthesis of nanoparticles by microorganisms and their applications. J. Nanomater. 270974.

Manivasagan, P., Oh, J., 2015. Production of a novel fucoidanase for the green synthesis of gold nanoparticles by *Streptomyces* sp. and its cytotoxic effect on HeLa cells. Mar. Drugs. 13, 6818–6837.

Marzouni, H.Z., Tarkhan, F., Aidun, A., Shahzamani, K., Tigh, H.R.J., Malekshahian, S., Lashgarian, H.E., 2018. Cytotoxic effects of coated gold nanoparticles on PC12 cancer cell. G.M.J. 8. e1110.

Mata, R., Nakkala, J.R., Sadras, S.R., 2016. Polyphenol stabilized colloidal gold nanoparticles from Abutilon indicum leaf extract induce apoptosis in HT-29 colon cancer cells. Colloids Surf. B Biointerfaces. 143, 499–510.

Mulvaney, P., 1996. Surface plasmon spectroscopy of nanosized metal particles. Langmuir 12, 788–800.

Musarrat, J., Dwivedi, S., Singh, B.R., Al-Khedhairy, A.A., Azam, A., Naqvi, A., 2010. Production of antimicrobial silver nanoparticles in water extracts of the fungus *Amylomycesrouxii* strain KSU-09. Bioresour. Technol. 101, 8772–8776.

Parasuraman, P., Antony, A.P., Lal, S.S.B., Sharan, A., Syed, A., Ahmed, M., Alarfaj, A.A., Busi, S., Maaza, M., Kaviyarasu, K., 2018. Antimicrobial photodynamic inactivation of fungal biofilm using amino functionalized mesoporus silica-rose bengal nanoconjugate against *Candida albicans*. Sci. Afr. 1.

Parasuraman, P., Antony, A.P., Lal, S.S.B., Sharan, A., Siddhardha, B., Kasinathan, K., Bahkali, N.A., Dawoud, T.M.S., Syed, A., 2019b. Antimicrobial photodynamic activity of toluidine blue encapsulated in mesoporous silica nanoparticles against *Pseudomonas aeruginosa* and *Staphylococcus aureus*. Biofouling 35 (1), 89–103.

Parasuraman, P., Anju, V.T., Lal, S.S.B., Sharan, A., Busi, S., Kasinathan, K., Arshad, M., Dawoud, T.M.S., Syed, A., 2019a. Synthesis and antimicrobial photodynamic effect of methylene blue conjugated carbon nanotubes on E. coli and S. aureus. Photochem. Photobiol. Sci. 18 (2), 563–576. https://doi.org/10.1039/C8PP00369F.

Park, H.Y., Park, S.H., Jeong, J.W., 2017. Induction of p53-Independent Apoptosis and G1 Cell cycle arrest by Fucoidan in HCT116 Human colorectal carcinoma cells. Mar. Drugs. 15, 154.

Raheman, F., Deshmukh, S., Ingle, A., Gade, A., Rai, M., 2011. Silver nanoparticles: novel antimicrobial agent synthesized from an endophytic fungus Pestalotia sp. isolated from leaves of Syzygiumcumini (L). NANO Biomed. Eng. 3, 174–178.

Rahme, K., Chen, L., Hobbs, R.G., Morris, M.A., O'Driscoll, C., Holmes, J.D., 2013. PEGylated gold nanoparticles: polymer quantification as a function of PEG lengths and nanoparticle dimensions. RSC Adv. 3, 6085–6094.

Rajkumari, J., Maria, Magdalane C., Siddhardha, B., Madhavan, J., Ramalingam, G., Al-Dhabi, N.A., Arasu, M.V., Ghilan, A.K.M., Duraipandiayan, V., 2019. Kaviyarasu K. Synthesis of titanium oxide nanoparticles using Aloe barbadensis mill andevaluation of its antibiofilm potential against Pseudomonas aeruginosa PAO1. J. Photochem. Photobiol., B.

Roopan, S.M., Priya, D.D., Shanavas, S., Acevedo, R., Al-Dhabi, N.A., Arasu, M.V., 2019. CuO/C nanocomposite: Synthesis and optimization using sucrose as carbon source and its antifungal activity. Mater. Sci. Eng., C 101, 404–414.

Shankar, S., Ahmad, A., Pasrichaa, A., Sastry, M., 2003. Bioreduction of chloroaurate ions by geranium leaves and its endophytic fungus yields gold nanoparticles of different shapes. J. Mater. Chem. 13, 1822–1826.

Sharif, M.K., Shah, F.-H., Butt, M.S., Sharif, H.R., 2017. Role of nanotechnology in enhancing bioavailability and delivery of dietary factors. Nanotechnol. Agri-Food Ind., 587–618

Singh, M., Kalaivani, R., Manikandan, S., 2013. Facile green synthesis of variable metallic gold nanoparticle using *Padinagymnospora*, a brown marine macroalga. Appl. Nanosci. 3, 145.

Sivakumar, A.S., Krishnaraj, C., Sheet, S., Rampa, D.R., Kang, D.R., Belal, S.A., Kumar, A., Hwang, I.H., Yun, S.I., Lee, Y.S., Shim, K.S., 2017. Interaction of silver and gold nanoparticles in mammalian cancer: as real topical bullet for wound healing- A comparative study *in vitro*. Cell. Dev. Biol. Anim. 53, 632–645.

Thangam, R., Kannan, S., Babu, S., Gunasekaran, P., Kaveri, K., Mohana, S., Kavita, A., Dhanagaran, D., Raja, S., 2011. Over expression of cyclooxygenase 2 detected in MCF-7 breast cancer cell and compared with lung carcinoma cellline (A549). Int. J. Biomed. Res. 2, 320.

Valsalam, S., Agastian, P., Arasu, M.V., Al-Dhabi, N.A., Ghilan, A.-K.M., Kaviyarasu, K., Ravindran, B.R., Chang, S.W., Arokiyaraj, S., 2019. Rapid biosynthesis and characterization of silver nanoparticles from the leaf extract of Tropaeolum majus L. and its enhanced in-vitro antibacterial, antifungal, antioxidant and anticancer properties. J. Photochem. Photobiol. B.

Valsalam, S., Agastian, P., Esmail, G.A., Ghilan, A.K.M., Al-Dhabi, N.A., Arasu, M.V., 2019.. Biosynthesis of silver and gold nanoparticles using Musa acuminata colla flower and its pharmaceutical activity against bacteria and anticancer efficacy. J. Photochem. Photobiol., B: Biol. https://doi.org/10.1016/j.jphotobiol.2019.111670.

Van de Weert, M., Haris, P.I., Hennink, W.E., Crommelin, D.J.A., 2001. Fourier transform infrared spectrometric analysis of protein conformation: effect of sampling method and stress factors. Anal. Biochem. 297, 160–169.

Verma, V.C., Singh, S.K., Solanki, R., Prakash, S., 2011. Biofabrication of anisotropic gold nanotriangles using extract of endophytic *Aspergillusclavatus* as a dual functional reductant and stabilizer. Nanoscale Res. Lett. 6, 1–7.

Vivek, R., Kannan, S., Achiraman, S., Thirumurugan, R., Ganesh, D.S., Krishnan, M., 2011. Surviving deficiency leads to imparalization of cytokinesis in cancer cells. Asian Pac. J. Cancer Prev. 12, 1675–1679.